Optics Letters

High-quality-factor multiple Fano resonances for refractive index sensing

Yuebian Zhang,[1] Wenwei Liu,[1] Zhancheng Li,[1] Zhi Li,[1] Hua Cheng,[1,2] Shuqi Chen,[1,2,*] and Jianguo Tian[1,2]

[1]The Key Laboratory of Weak Light Nonlinear Photonics, Ministry of Education, School of Physics and TEDA Institute of Applied Physics, Nankai University, Tianjin 300071, China
[2]The Collaborative Innovation Center of Extreme Optics, Shanxi University, Taiyuan, Shanxi 030006, China
*Corresponding author: schen@nankai.edu.cn

Received 31 January 2018; revised 15 March 2018; accepted 16 March 2018; posted 19 March 2018 (Doc. ID 321077); published 11 April 2018

We design and numerically analyze a high-quality (Q)-factor, high modulation depth, multiple Fano resonance device based on periodical asymmetric paired bars in the near-infrared regime. There are four sharp Fano peaks arising from the interference between subradiant modes and the magnetic dipole resonance mode that can be easily tailored by adjusting different geometric parameters. The maximal Q-factor can exceed 10^5 in magnitude, and the modulation depths ΔT can reach nearly 100%. Combining the narrow resonance line-widths with strong near-field confinement, we demonstrate an optical refractive index sensor with a sensitivity of 370 nm/RIU and a figure of merit of 2846. This study may provide a further step in sensing, lasing, and nonlinear optics.

OCIS codes: (160.3918) Metamaterials; (260.5740) Resonance; (280.4788) Optical sensing and sensors.

https://doi.org/10.1364/OL.43.001842

High-quality (Q)-factor resonators play a key role in various fields of applications, such as nonlinear optics [1], sensors [2,3], lasers [4], chiral optical response [5], and optical switching [6]. The Fano resonance is one effective method to realize the high Q-factor resonance in metamaterials and metasurfaces [7,8]. The physical origin of Fano resonances can be attributed to the interference of a continuum (or broad) state and a discrete (or narrow) state. They are often characterized by asymmetric spectral line profiles, instead of typical symmetric line shapes in isolated single resonances [7–10]. Under certain conditions, the Fano resonance can be regarded as the classical analogue of electromagnetically induced transparency (EIT) [7]. More specifically, when the frequency detuning between the broad resonance and narrow resonance becomes sufficiently small, the destruction between the two resonances will result in a narrow transparency window at the broad transmission dip, leading to the EIT-like transmission peak. Over the past few years, the Fano resonance has been observed in a number of nanoscale classical oscillator systems enabled by plasmonic nanostructures [8,10–12], which were fabricated from metals. However, owing to the Ohmic losses, it is difficult to obtain high Q-factor Fano resonances at infrared and optical frequencies by using plasmonic nanostructures.

Recently, some new strategies based on dielectric structures have been developed to achieve high Q-factor Fano resonances [13–16]. The metasurface transmission and reflection spectra resulting from such an approach featuring Fano resonances can be much narrower than the traditional plasmonic metasurface due to the avoiding of Ohmic losses. In addition, dielectric structures can support both electric and magnetic dipolar Mie-type resonances [17]. So, they can easily realize magnetic Fano resonance [18,19], in which the fundamental resonance mode is a magnetic mode. Moreover, recent works show that the dielectric structures can support toroidal dipole (TD) resonance, which is characterized by currents flowing on the surface of a torus or a series of magnetic dipoles aligned along enclosed paths [20–22]. In particular, when an electric dipole (ED) resonance and a TD resonance are overlapped with the same scattering magnitude but are out of phase, they can produce the nonradiating anapoles [23,24], which can be used to realize high Q-factor resonances [25,26]. As a result of the different applications, the research interest in optical Fano resonances has extended from single Fano resonance to multiple Fano resonances [27,28]. Multiple Fano resonances can be widely used in multiwavelength surface enhanced spectroscopy, multichannel biosensors, and multiband slow-light devices. In particular, recent work has shown that multiple Fano resonances are also very useful in enhancing multiband second harmonic generation [1], in which different Fano resonances match different fundamental harmonic wavelengths and different second harmonic wavelengths. But so far, there are few studies that can realize more than three high Q-factor Fano resonances at the same time. And the modulation depths ΔT, defined as the transmission intensity differences between the Fano peaks and the Fano dips $T_{\text{peak}} - T_{\text{dip}}$, always decrease with the increase of the Q-factors. Thus, there is a significant benefit to realize multiple Fano resonance devices with a high Q-factor and high modulation depth.

In this Letter, we demonstrate a high Q-factor, high modulation depth, multiple Fano resonance device based on periodical asymmetric paired bars (APBs). There are four sharp Fano peaks, which can be easily tailored by adjusting different geometric parameters. The maximal Q-factor can exceed 10^5 in magnitude, and the modulation depths ΔT can reach nearly 100%. Combining the narrow resonance line-widths with strong near-field confinement, we theoretically demonstrate an optical refractive index sensor with a sensitivity (S) of 370 nm/RIU and a figure of merit (FOM) of 2846. This study may provide a further step in the development of sensing, lasing, and nonlinear optics.

The designed multiple Fano resonance device based on periodic APBs is shown in Fig. 1. The periods along x and y axes are P_x and P_y, respectively, which are set $P_x = P_y = P$. The unit cell of the APBs is composed of two Si bars on glass substrate with slightly different widths, w_1 and w_2. The asymmetry parameter δ is defined as $\delta = w_1 - w_2$. The paired bars are positioned in parallel with a gap g. The length of the Si bar is L and the thickness is t. The incident plane wave has an electric field polarized along the x direction with a propagation vector along the z direction, as shown in Fig. 1(a). Numerical simulations are conducted using both the finite-element-method-based commercial software COMSOL Multiphysics 4.3 [29] and the finite-difference time-domain (FDTD) approach based on the commercial software package Lumerical Solutions. The optical constants of amorphous Si and glass were taken from Ref. [30].

Figure 2(a) shows the transmission spectra of the proposed metasurface at different asymmetry parameter δ when $P = 650$ nm, $t = 260$ nm, $L = 480$ nm, $g = 80$ nm, and $w_1 + w_2 = 400$ nm. When $w_1 = w_2 = 200$ nm, a broad resonance dip is observed around the wavelength of 1225 nm, with an EIT-like transmission peak appearing at 1186.4 nm. To get insight into the origin of this EIT-like peak, we calculated the three dominant Cartesian multipole moments around the resonance wavelength when $\delta = 0$. There are two dominant resonance modes, TD and magnetic dipole (MD) resonances, at the transmission peak, as shown in Fig. 2(b), indicating that the EIT-like transmission peak is mostly due to the interference between the MD resonance and the TD resonance. This EIT-like resonance effect can be viewed as a special case of Fano resonance. In addition, the amplitudes of the current Cartesian ED moment $|P_x|$ and the TD moment $|ikT_x|$ are equal at about 1191.5 nm. Their phase difference $|\varphi(P_x) - \varphi(ikT_x)|$ is approximately equal to π [Fig. 2(c)]. As a result, the far-field radiation of the ED and TD resonances will interfere destructively with each other, corresponding to the anapole mode [23–26]. When $w_1 = 210$ nm and $w_2 = 190$ nm, three additional Fano resonance peaks appear at 1113.2 nm (P1), 1161.6 nm (P2), and 1302.6 nm (P3), respectively. The EIT-like peak undergoes a slight red shift. Figure 2(d) shows the Q-factors of the four resonance modes with different asymmetry parameter δ. The Q-factor is calculated as a ratio between the resonant wavelength λ_0 and the full width at half-maximum (FWHM) $\Delta\lambda$ of a resonant peak. For the Fano resonances with asymmetric line shapes, the resonant region lies between the dip and peak wavelengths, λ_d and λ_p, corresponding to the destructive and constructive interferences, respectively. Therefore, we adopt $|\lambda_d - \lambda_p|$ as the FWHM of a Fano resonance. It can be seen that the Q-factor of the TD peak will increase with the increase of asymmetry parameter δ, as shown in Fig. 2(b). However, for P1, P2, and P3, the Q-factors can be increased by reducing the asymmetry parameter. When $\delta = 5$ nm, the Q-factors of P1, P2, and P3 can reach about 2.8×10^4, 2.9×10^4, and 1.3×10^5, respectively.

To gain insight into the nature of the designed multiple Fano resonance device and identify the subradiant modes related to the Fano resonances, we calculated the electric field and magnetic field distributions at different resonance modes when $\delta = 20$ nm, as shown in Fig. 3. The electric field and magnetic field are normalized to the incident electromagnetic field. At the wavelength of 1225 nm, we can see that the electric field in the $x - z$ plane forms a loop, whereas the magnetic field in the $x - y$ plane is almost linearly polarized along the y axis, corresponding to a MD resonance mode. At the wavelength of 1193.2 nm, the magnetic field in the $y - z$ plane forms a loop, and the electric field in the $x - y$ plane forms two reversed loops, indicating that it is a TD resonance mode [20–22,31]. At P1 resonance mode, the magnetic field in the two Si bars has

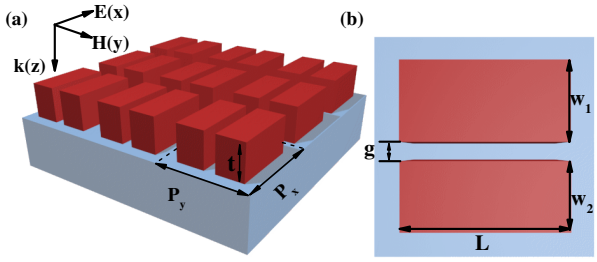

Fig. 1. (a) Schematic of the dielectric metasurface composed of periodical asymmetric Si nanobar pairs on silica substrate and the incident light polarization configuration. (b) Top view and geometric parameters of a unit cell of the Si bar pairs.

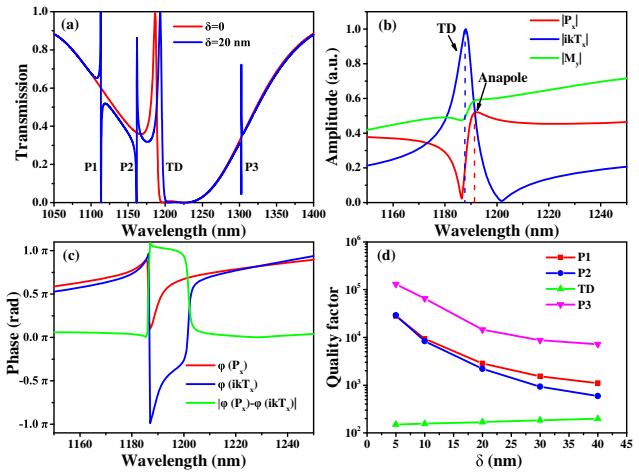

Fig. 2. (a) Transmission spectra of the metasurface at different asymmetry parameter δ when $P = 650$ nm, $t = 260$ nm, $L = 480$ nm, $g = 80$ nm, and $w_1 + w_2 = 400$ nm. (b) Amplitude of the Cartesian electric dipole moment $|P_x|$, toroidal dipole moment $|ikT_x|$, and magnetic dipole moment $|M_y|$ around the TD resonance wavelength when $\delta = 0$. (c) The phases as well as their difference of P_x and ikT_x. (d) The quality factors of the four resonance modes with different asymmetry parameter δ.

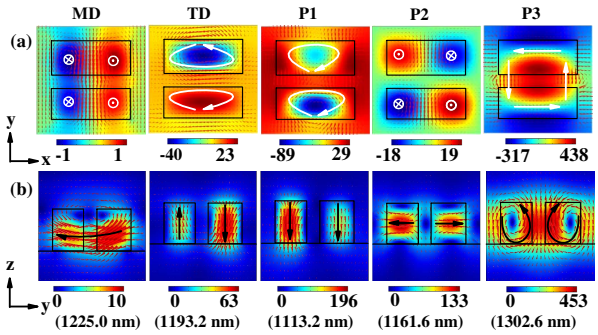

Fig. 3. (a) Normalized electric field and magnetic field distributions at different resonance modes in the $x-y$ plane bisecting the nanobars. The color maps at MD and P2 (TD, P1, and P3) resonance modes represent $E_z(H_z)$ distributions. The red cones at MD and P2 (TD, P1, and P3) resonance modes represent magnetic field (electric field) vector distributions. The white arrows show the electric field directions. (b) Normalized magnetic field amplitude distributions $|H/H_0|$ (color maps) and magnetic field vector distributions (red cones) at different resonance modes in the $y-z$ plane bisecting the nanobars. The black arrows show the magnetic field directions.

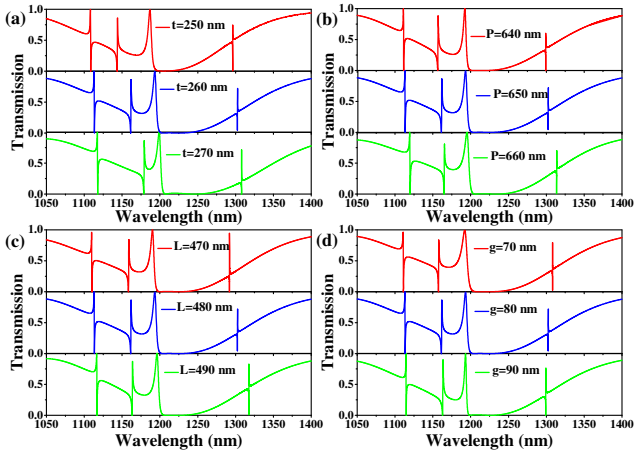

Fig. 4. Dependence of the transmission spectra for different geometric parameters when $\delta = 20$ nm. (a) Transmission spectra for different t. (b) Transmission spectra for different P. (c) Transmission spectra for different L. (d) Transmission spectra for different g.

the same direction and is almost linearly polarized along the z axis in the $y-z$ plane. At the same time, the electric field in the $x-y$ plane forms two loops rotating in the same direction. As a result, this resonance mode can radiate like two parallel magnetic dipoles oriented along the z axis. At P2 resonance mode, the magnetic field in the two Si bars oriented along the y axis in the $y-z$ plane but with opposite direction. At the same time, the electric field in the $x-z$ plane forms two reversed loops. This resonance mode can be regarded as a magnetic quadrupole (MQ) resonance. At P3 resonance mode, the electric field in the $x-y$ plane forms a loop, and the magnetic field in the $y-z$ plane forms two reversed loops. In addition, unlike other resonance modes whose magnetic field is mainly localized in the dielectric bars, the magnetic field of P3 resonance mode is mainly localized in the gap, and the normalized magnetic field amplitude $|H/H_0|$ can be enhanced by more than 450 times, comparable to plasmonic nanostructures.

To study the dependence of the transmission spectra on different geometric parameters, we applied the transmission spectra to different geometric parameters when $\delta = 20$ nm in Fig. 4. Other geometric parameters are the same as the parameters used in Fig. 2(a) except the variable parameter shown in each figure. From Figs. 4(a)–4(c), it can be seen that the Fano peaks redshift as the thickness t, the period P, or the length L increases. P2 is more sensitive to t, and P3 is more sensitive to L, while P1 and the TD peak are less sensitive to these parameters. If the lattice period is changed, P3 will have the biggest wavelength shift. This indicates that the collective oscillations of the array play an important role in the forming of P3 but have little impact on the TD peak. When the gap g increases from 70 nm to 90 nm, P1 and P2 have a slight redshift while P3 undergoes a blueshift, as shown in Fig. 4(d). The TD peak position remains nearly unchanged, but its line-width becomes narrow with the increase of g. The reason is that coupling coefficient between the TD resonance and the MD resonance is reduced with the increase of g [26,32]. Thus, the multiple Fano resonances can be easily tailored by adjusting different geometric parameters.

As an example of applications, we proved a refractive index sensor based on the proposed metasurface. The geometric parameters of the refractive index sensor are $\delta = 20$ nm, $P = 650$ nm, $t = 260$ nm, $L = 400$ nm, $g = 100$ nm, and $w_1 + w_2 = 400$ nm, respectively. Figure 5(a) shows the transmission spectrum of the asymmetric structure on silica substrate, whose surface is covered by liquids with a refractive index of 1.3330. The liquid is assumed to fill the gaps and cover the top of the Si bars. It can be seen that the transmission spectrum exhibits four sharp Fano resonance peaks with near-unity modulation depths. Optically resonant sensors are characterized by both the line-width of the resonance ($\Delta\lambda$) as well as the shift in the resonance per refractive-index-unit change (S). These two values comprise the FOM that is given by FOM $= S/\Delta\lambda$. Figures 5(b)–5(d) show the transmission

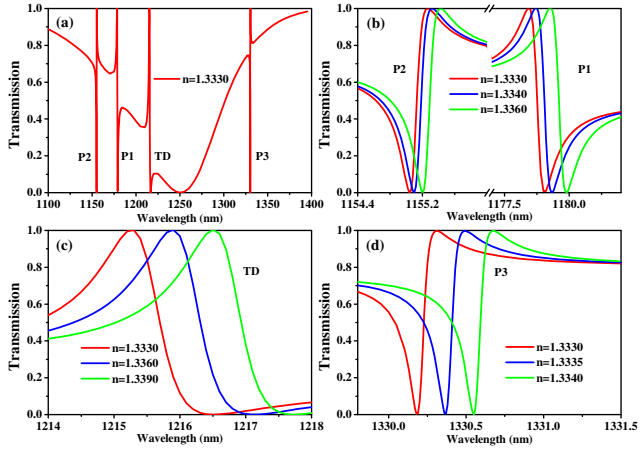

Fig. 5. (a) Transmission spectrum of the asymmetric structure on silica substrate and covered by liquids with a refractive index of 1.3330. (b)–(d) Transmission spectra of the four resonance modes when the structure was covered by liquids with different refractive indexes.

spectra of the four resonance modes when the structure was covered by liquids with different refractive indexes. It can be seen that a substantial movement in the peak position is realized despite the small index change. The averaged sensitivities are about 53 nm/RIU, 300 nm/RIU, 200 nm/RIU, and 370 nm/RIU for P2, P1, TD, and P3, respectively. Considering their narrow line-widths, the FOM of P2, P1, TD, and P3 can reach 241, 462, 167, and 2846, respectively. The differences in the sensitivity of different modes are mainly due to the field distributions. As shown in Fig. 3, at P3 resonance mode, the electric field and magnetic field are mainly localized in the gap, while the electric field and magnetic field of P2 resonance mode are mainly localized in the dielectric bars. As a result, the P3 resonance mode is more sensitive to the changes of the surroundings, and P2 resonance mode is less sensitive to them. Although the Fano peaks have a blueshift when the thickness of liquid decreases to below 400 nm, the line shape and modulation depth change little when the thickness of liquid decreases to 260 nm. That is to say, the amount of liquid required just needs to submerge the nanostructure. The high FOM and near-unity modulation depths of these Fano peaks offer a promising opportunity to design a high-performance refractive index sensor device.

In conclusion, a high Q-factor, high modulation depth, multiple Fano resonance device is demonstrated. There are four Fano peaks—P1, P2, TD, and P3. The Q-factors of P1, P2, and P3 can reach about 2.8×10^4, 2.9×10^4, and 1.3×10^5 when the asymmetry parameter is $\delta = 5$ nm. The intrinsic multimodal response and the sharp peaks make this structure suitable for refractive index sensing. The sensitivity and FOM of the proposed device can reach 370 nm/RIU and 2846 when $\delta = 20$ nm. We can get a higher Q-factor and further improve the FOM by reducing the asymmetry parameter. In addition, the normalized magnetic field amplitude $|H/H_0|$ can be enhanced by more than 450 times at the P3 resonance mode. This strongly enhanced magnetic field in the surrounding substance allows the metasurface to serve as an ideal platform for enhancing interaction with the surrounding medium. It is also worth noting that the multiple Fano resonances can be easily tailored by adjusting different geometric parameters, making it more adaptable to potential applications. This platform can be easily integrated with microfluidic systems for lab-on-a-chip applications. In view of the potential applications of Fano resonances in optoelectronic devices, they may find numerous applications ranging from nonlinear optics and sensing to the realization of new types of optical modulation and low-loss slow-light devices.

Funding. National Key Research and Development Program of China (2017YFA0303800, 2016YFA0301102); National Natural Science Foundation of China (NSFC) (11774186, 11574163, 61378006); Natural Science Foundation of Tianjin City (16JCQNJC01700); 111 Project (B07013).

REFERENCES

1. S.-D. Liu, E. S. P. Leong, G.-C. Li, Y. Hou, J. Deng, J. H. Teng, H. C. Ong, and D. Y. Lei, ACS Nano **10**, 1442 (2016).
2. M. Gupta and Y. K. Srivastava, Appl. Phys. Lett. **110**, 121108 (2017).
3. Y. Tao and Z. Guo, Ann. Phys. **529**, 1600259 (2017).
4. N. I. Zheludev, S. L. Prosvirnin, N. Papasimakis, and V. A. Fedotov, Nat. Photonics **2**, 351 (2008).
5. C. Wu, N. Arju, G. Kelp, J. Fan, J. Dominguez, E. Gonzales, E. Tutuc, I. Brener, and G. Shvets, Nat. Commun. **5**, 3892 (2014).
6. C. Argyropoulos, Opt. Express **23**, 23787 (2015).
7. B. Luk'yanchuk, N. I. Zheludev, S. A. Maier, N. J. Halas, P. Nordlander, H. Giessen, and C. T. Chong, Nat. Mater. **9**, 707 (2010).
8. Z.-J. Yang, Z.-H. Hao, H.-Q. Lin, and Q.-Q. Wang, Nanoscale **6**, 4985 (2014).
9. U. Fano, Phys. Rev. **124**, 1866 (1961).
10. Z. Liu, Z. Liu, J. Li, W. Li, J. Li, C. Gu, and Z. Li, Sci. Rep. **6**, 27817 (2016).
11. X. Tian, Y. Fang, and B. Zhang, ACS Photon. **1**, 1156 (2014).
12. Z. Fang, J. Cai, Z. Yan, P. Nordlander, N. J. Halas, and X. Zhu, Nano Lett. **11**, 4475 (2011).
13. G. Sun, L. Yuan, Y. Zhang, X. Zhang, and Y. Zhu, Sci. Rep. **7**, 8128 (2017).
14. W. X. Lim, S. Han, M. Gupta, K. F. MacDonald, and R. Singh, Appl. Phys. Lett. **111**, 061104 (2017).
15. D.-J. Cai, Y.-H. Huang, W.-J. Wang, W.-B. Ji, J.-D. Chen, Z.-H. Chen, and S.-D. Liu, J. Phys. Chem. C **119**, 4252 (2015).
16. J. Zhang, W. Liu, Z. Zhu, X. Yuan, and S. Qin, Opt. Express **22**, 30889 (2014).
17. J. C. Ginn, I. Brener, D. W. Peters, J. R. Wendt, J. O. Stevens, P. F. Hines, L. I. Basilio, L. K. Warne, J. F. Ihlefeld, and P. G. Clem, Phys. Rev. Lett. **108**, 097402 (2012).
18. K. E. Chong, B. Hopkins, I. Staude, A. E. Miroshnichenko, J. Dominguez, M. Decker, D. N. Neshev, I. Brener, and Y. S. Kivshar, Small **10**, 1985 (2014).
19. B. Hopkins, D. S. Filonov, A. E. Miroshnichenko, F. Monticone, A. Alú, and Y. S. Kivshar, ACS Photon. **2**, 724 (2015).
20. W. Liu and Y. S. Kivshar, Philos. Trans. R. Soc. London A **375**, 20160317 (2017).
21. W. Liu, J. Shi, B. Lei, H. Hu, and A. E. Miroshnichenko, Opt. Express **23**, 24738 (2015).
22. N. Papasimakis, V. A. Fedotov, V. Savinov, T. A. Raybould, and N. I. Zheludev, Nat. Mater. **15**, 263 (2016).
23. A. E. Miroshnichenko, A. B. Evlyukhin, Y. F. Yu, R. M. Bakker, A. Chipouline, A. I. Kuznetsov, B. Lukyanchuk, B. N. Chichkov, and Y. S. Kivshar, Nat. Commun. **6**, 8069 (2015).
24. L. Wei, Z. Xi, N. Bhattacharya, and H. P. Urbach, Optica **3**, 799 (2016).
25. A. A. Basharin, V. Chuguevsky, N. Volsky, M. Kafesaki, and E. N. Economou, Phys. Rev. B **95**, 035104 (2017).
26. S.-D. Liu, Z.-X. Wang, W.-J. Wang, J.-D. Chen, and Z.-H. Chen, Opt. Express **25**, 22375 (2017).
27. J. Zhang, K. F. MacDonald, and N. I. Zheludev, Opt. Express **21**, 26721 (2013).
28. S. Campione, S. Liu, L. I. Basilio, L. K. Warne, W. L. Langston, T. S. Luk, J. R. Wendt, J. L. Reno, G. A. Keeler, I. Brener, and M. B. Sinclair, ACS Photon. **3**, 2362 (2016).
29. *COMSOL Multiphysics User's Guide, Version 4.3* (Comsol AB, 2012).
30. E. D. Palik, *Handbook of Optical Constants of Solids* (Academic, 1985), Vol. **I**.
31. Z. Liu, S. Du, A. Cui, Z. Li, Y. Fan, S. Chen, W. Li, J. Li, and C. Gu, Adv. Mater. **29**, 1606298 (2017).
32. Y. Yang, I. I. Kravchenko, D. P. Briggs, and J. Valentine, Nat. Commun. **5**, 5753 (2014).